Regular Article

Zainab Shakir Radeef*

# Design and characteristics of two-dimensional piezoelectric nanogenerators

https://doi.org/10.1515/eng-2022-0409
received June 28, 2022; accepted January 25, 2023

**Abstract:** In the last decades, increasing interest in piezoelectric material has opened new horizons in electronic industries and alternative energy fields. In this study, a piezoelectric (ZnO NSs–$Na_2Ti_6O_{13}$) were prepared from Zinc Oxid Nanosheets (ZnO NSs) and Disodium Hexa titanate (NTO). The dielectric, harvester performance, and the pyroelectric effect of ZnO NSs – NTO explored experimentally. Under different experimental conditions and mechanisms, the generated voltages had been measured where a quasi-static pressing force was applied at the harvester. In addition, the derived voltage has been rectified when the harvester was mounted over a cantilever beam, where the power density was $0.10 \pm 0.1\,mW/cm^3$. Finally, there was further investigation of the pyroelectric property which yielded a maximum pyroelectric coefficient of $30.51\,\mu C/m^2\,°C$ at low temperature.

**Keywords:** energy harvesting, heterojunction, piezoelectric, ZnO, pyroelectric, sodium titanate

## 1 Introduction

Piezoelectric materials are attractive as they possess a high sensitivity to mechanical vibration and are capable to convert the waste vibrations to useful electrical energy as well as storing it for later use. These materials are physically distinguished by having a direct and reverse property whereas when the material is excited by mechanical vibration energy, this energy can convert to electrical power and *vice versa*. Additionally, the use of pyroelectric materials also has a considerable interest where the heat is extremely difficult to recover from low-grade waste sources. Outstanding advances have been achieved in manufacturing piezoelectric transducers and actuators where most applications are formed from soft Lead–Zirconate–Titanate (PZT) to several other ferroelectric and non-ferroelectric materials. Recently, the fabrication of piezoelectric nanogenerators has had wide separation [1,2]. Since clean energy sources are sorely needed, numerous harvesting techniques have been developed to generate optimal energy based on the use of a PZT harvester. The optimal excreting of power derived by different harvesting mechanisms such as excited cantilever beam to harvest the highway-traffic excitations [3], customized materials [4], using a series of connected banders [5], a customized geometry [6], flexible films [7], high mechanical excitations amplitude [8], and harvesting mechanism smart rectification of the extracted power [9]. The piezoelectric materials that have ferroelectric manners such as PZT, $PbZrTO_3$, $BrTiO_3$, $LiNbO_3$, and PVDF to many other components are distinguished by their fast electrical response and high figures of merit [10]. The required power density for powering wireless node is 1 mW with long-term durability and ability to transmit long distances [11,12]. Several piezoelectric materials can detect any change of temperature, whereas pyroelectric materials can also convert heat into electricity. Among the pyroelectric materials, aluminum nitride (AlN) and zinc oxide (ZnO) exhibit dual-generation functions. Zinc Oxide was recognized by its non-ferroelectric characteristic; it is a promising material and could be used in thermoelectric applications [13]. ZnO NG has been received a remarkable improvement in piezoelectricity where the piezoelectric coefficient is recorded in the range of 25–34 pm/V, and the average AC-voltage generated was between 0.1 and 2 volts [14–18]. Nanoscale growth exhibits a variety of configurations where the nanostructured zinc oxide can be tailored its morphology structure to suit any application. It is crucial to control the crystal growth percentage, morphological shape, and crystal orientation through synthetic methods and experimental conditions. Prior to this study, a wide range of ZnO NG morphologies were investigated such as nanotubes [19], nanofibers [20], nanosheets [21], nanorings, nanowires [22], nanobelts [23], and nanoflowers [24]. It was found that the

* **Corresponding author: Zainab Shakir Radeef,** Department of Materials Engineering, Faculty of Engineering, University of Kufa, Najaf, Iraq; Nanotechnology and Advanced Materials Research Unit (NAMRU), Faculty of Engineering, University of Kufa, Najaf, Iraq, e-mail: zina_engi@um.edu.my, zainab.aldulaimi@uokufa.edu.iq, tel: +964-7830030456

short circuit current was in the range of nanoamps to several microamps [14]. Generally, a low-dimensional material is classified according to the dimensions of its crystallization morphology. In more detail, nanoparticles (0D) have zero-dimensional growth, and the material is called one-dimensional (1D) such the nanofibers, nanotubes, and nanowires. Likewise, crystallization involving two dimensions results in a 2D nanostructure. The performance of 0D, 1D, and 2D materials were compared experimentally. Excellent performance and higher efficiency were found in ZnO-nanosheets, the generated power was in the range of 2.4 $\mu W/m^2$ whereas the 1D and 2D nanogenerators provided 0.12 and 1.3 $\mu W/m^2$, respectively [25]. Hydrothermal preparation of two-dimensional ZnO (2D NSs) and the performance has been compared with ZnO nanowires (1D NWs). In terms of current output, the performance is far superior to 1D NWs where the 2D NSs were nearly fourfold more effective [26]. Nanosheets are among the best materials for wearable devices, ZnO NSs display a large surface-to-volume ratio and thus are light and offer excellent electrochemical, biocompatible, and superior sensing properties [27].

Self-rectification of signal output has been implemented as another harvesting mechanism, where rectification of signal output was obtained by using ZnO nanosheets doped with vanadium (V). The formation mechanism of ZnO NSs involves the fabrication of ZnO NWs, where the zinc ions $Zn^{2+}$ and $O^{2-}$ ions are attracted alternatively along the *c*-axis of NWs, and when the growth forward *c*-axis is suppressed, the nanosheets configured by transforming the ZnO NWs to ZnO NSs [28]. From other perspectives, ZnO is one of the fundamental materials for developing multifunctional semiconductors, which is recognized as one of the n-type semiconductors. Specifically, there was the existence of intrinsic defects such as O vacancies O(V) that have more electrons in the atomic outer shell [29]. A half rectification of ac signal was observed as a response to the heat exposure, and a positive dc rectifying current is generated as a result of the formation of a p–n heterojunction [30]. In addition to the pyroelectricity, ZnO has fast photoresponse with large broadband. It found that an instantaneous polarization occurs when temperature increases rapidly under the light. A group of researchers had developed a hybrid pyroelectric and photovoltaic photodetector sensor from n-ZnO/p-Zn Te heterojunction materials, the device exhibited rapid responses to light and wideband response when the temperature increased. There were broad rectifications of the current at voltages between 1.5 and 1.8 [31].

Piezoelectric harvesters that are lead-free have recently gained popularity, sodium titanate (NTO) was combined with other materials such as ($NaBiTiO_3$–$BaTiO_3$), hence it produces excellent electromechanical properties. The piezoelectric coefficients ($d_{33}$) of $NaBiTiO_3$–$BaTiO_3$ reconducted under different experimental conditions varied between 153 and 216 pC/N [32]. It was found that the NTO has desire crystalline structure, excellent chemical stability, excellent cyclic stability, and high conductivity characteristics. NTO was used as ion exchangers [33,34], energy harvest sensors, photocatalysis, sensors [35], and biomedical applications. The raw materials of NTO have widespread abundance, affected manufacturing cost, low toxicity, and are useful for numerous applications; it was used as charge storage material and serves as a positive terminal that attracts the majority carriers of the material [36]. The generated voltage varies and depends on the applied mechanical stress where the dynamic characteristics (i.e., natural frequency, damping rate, and mode shape) must consider for optimal output. The integration of harvesters and beams for harvesting energy has been widely studied where the dynamic characteristics of harvesters and their host structures have to be matched [37]. In this article, ZnO NSs–NTO were hydrothermally synthesized and compacted between two electrodes. The optimization of dielectric properties is realized due to the presence of an NTO layer that has a narrow energy gap. In previous studies, the ZnO NSs were used to generate voltage by pressing and releasing mechanisms. As a result, this study examines the voltage output over a cantilever as well. The response of ZnO NSs–NTO to different mechanical excitations has been explored (e.g., it was examined at selected point over a cantilever beam and with finger pressing). Upon full rectification of the signal, the derived power could be used to illuminate a light-emitting diode (LED). In addition, pyroelectricity was observed at low temperatures between 35 and 25°C.

# 2 Experiment setup and procedure

## 2.1 Sample preparation

The raw materials for synthesized ZnO NSs–NTO were Zn ($CH_3COO$), Sodium Hydroxide, and Titanium Dioxide (the purity of Titanium Dioxide was 99.5% purity). The materials have been purchased from R Essex U.K.). NTO was prepared by using a solution gel method, where NaOH–$TiO_2$ mixture was prepared with a molar ratio of 1: 0.5. The first step to prepare the ZnO NSs was by using a heavy stirring of precursor solution that consists of zinc acetate ($Zn(CH_3COO)_2$–$2H_2O$) and $C_6H_{12}N_4$ with an equimolar ratio of 0.03 M, the precursor solution stirred for 2 h at 80°C. The reaction produced a white precipitate which was filtered

using a fine filter paper and washed twice with deionized water.

The obtained solution (wet powder) was applied above the zinc electrode with a thin film applicator and dried at 100°C for 30 min. A layer from NTO suspension was applied above the ZnO layer to be as a positive terminal, and then, the sample was left to dry. The Cu sheets were set up over the NTO layer, a thermal treatment process was carried up at 60°C for 15 min. Lastly, the sample was pressed and packaged with PET sheets for further damage prevention. Figure 1 illustrates the configuration of the ZnO NSs–NTO harvester.

## 2.2 Energy harvesting procedure

For harvesting energy, the harvester was mounted on a cantilever beam and excited by an electric shaker to produce a cyclic excitation at a frequency of 30 Hz. The DC and AC outputs were measured. The test rig setup is illustrated in Figure 2. The dynamic characteristics of the beam were analyzed based on the experimental Modal Analysis (MA) and Operational Deflection Shape (ODS). It was found that the mode shape of the beam was in linear distribution at the natural frequency of 30 Hz where nine discrete points have been assigned over the cantilever, and point 3 (strained region) was the selected point in this study. The generated AC voltage was measured using NI USB-9162 hardware, and the excitation of the cantilever was detected by Pocket Laser Tachometer (Monarch PLT200). Alternative signals were rectified and converted to a DC signal by using a voltage regulator circuit consisting of four Schottky diode bridges (1N5817) and the rectified current was stored at 100 μF. The storage energy was efficiently operated a light emission diode (5 mm).

# 3 Result and discussion

## 3.1 Surface analysis and crystalline structure

The nanostructure morphology of ZnO NSs–NTO was investigated by Field Emission Scanning Electron Microscopy (FESEM); the ZnO NSs and the NTO columns are illustrated in Figure 3. The FESEM morphology images were analyzed by Image J software. Morphologically, the thickness of the ZnO NSs was an average of 28.2 nm, which makes it one of the thinnest known materials [38].

The output current increased by increasing the area of the nanosheets and reducing the sheets thickness [26]. The morphology of the ZnO was detected by FESEM, and ZnO NSs were grown with a thickness average of 28.2 nm. Where a good piezoelectric property could be realized when the grown nanosheets are extremely slim and have a large area [26]. The morphology of NTO configured as columns in microscale size; the mean rate of columns' lengths was about 17.55 μm whereas the formed columns

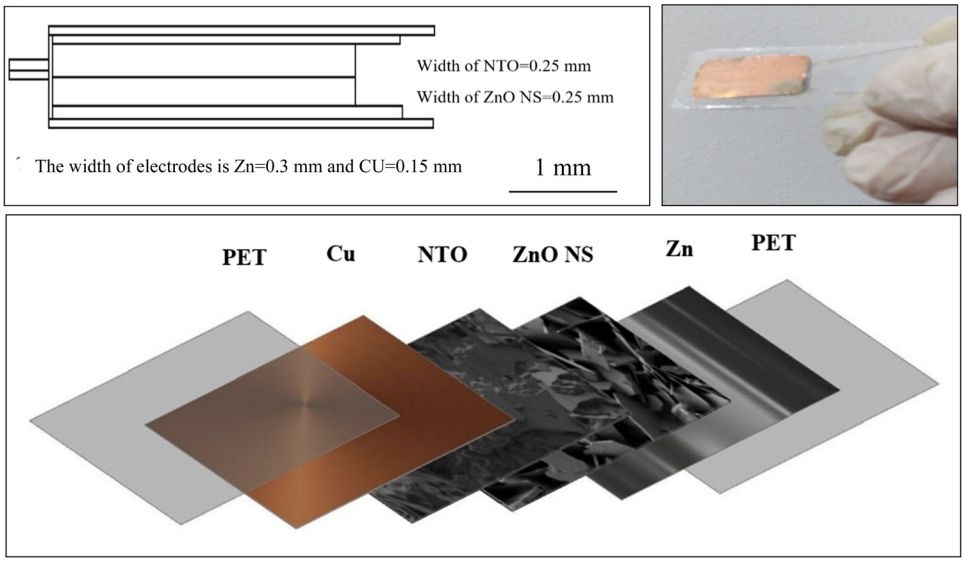


**Figure 1:** Construction of ZnO NSs–NTO harvester.

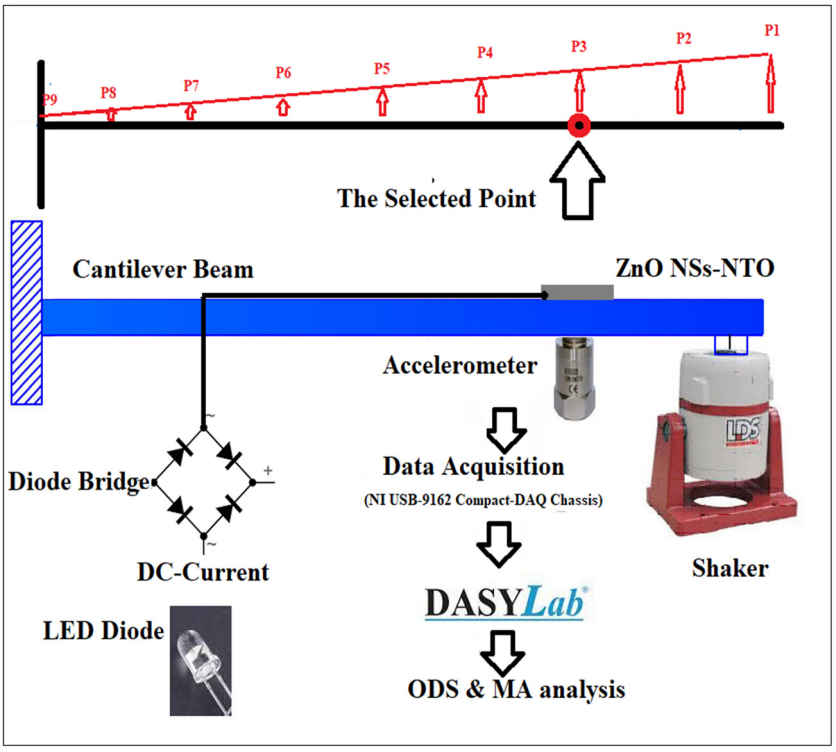


**Figure 2:** Experimental setup of excited beam cantilever.

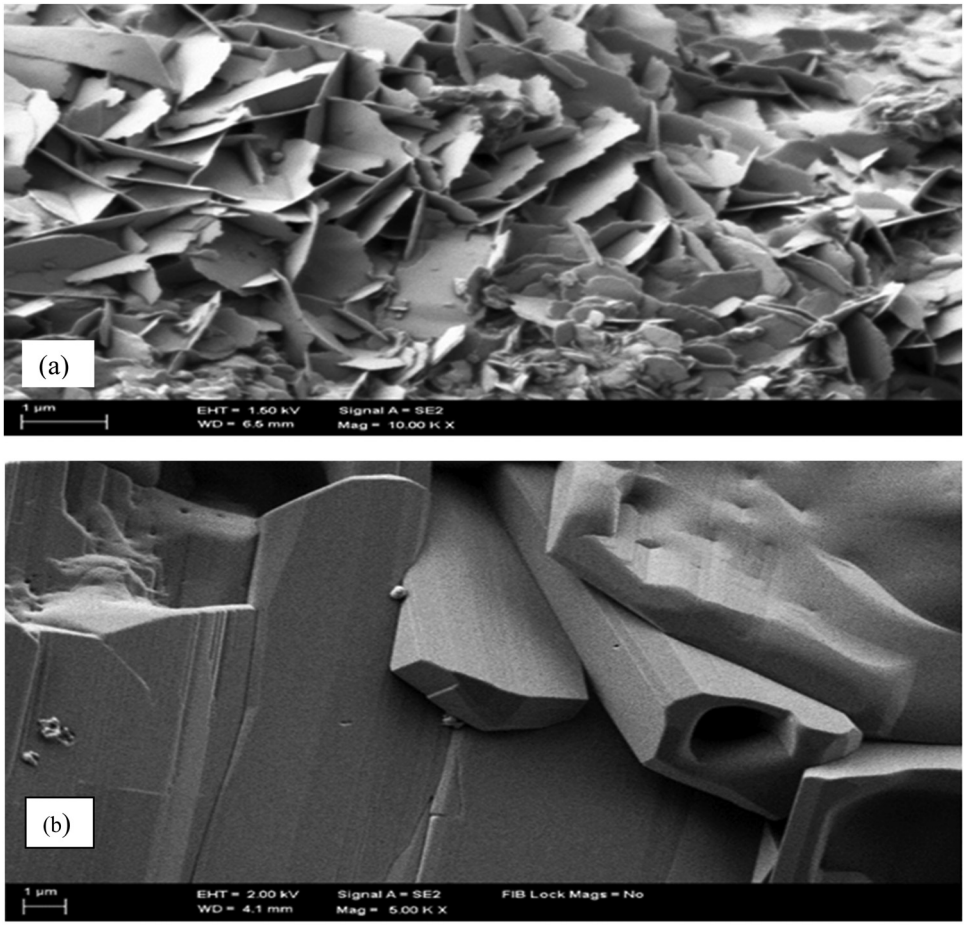


**Figure 3:** Structure of ZnO NSs–NTO: (a) zinc nanosheets layer; (b) disodium hexatitanate layer.

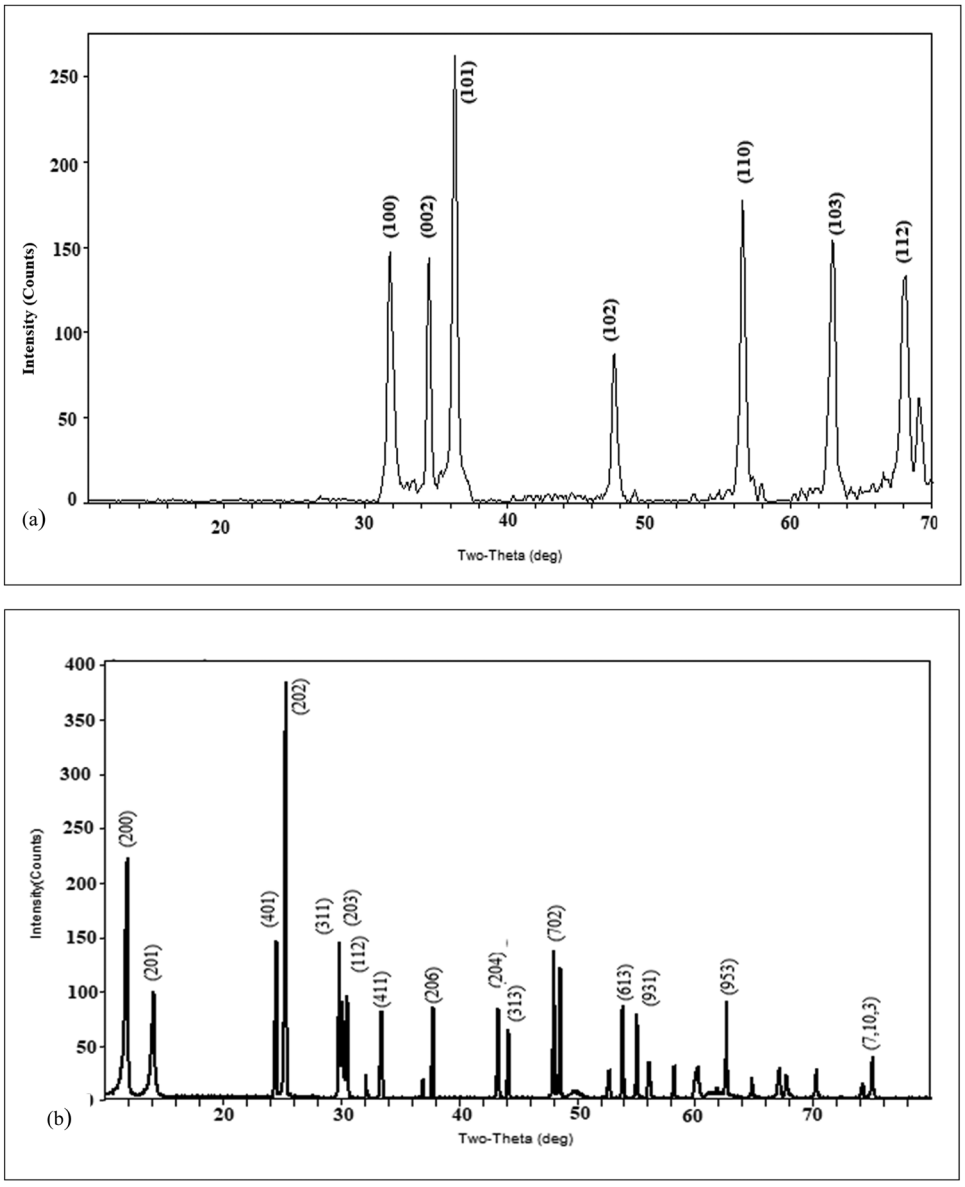


**Figure 4:** X-Ray diffraction: (a) ZnO NSs spectrum; (b) NTO spectrum.

had a cavity with an area of 3.63 μm$^2$. The lattice structure of ZnO NSs and NT was analyzed. A PANalytical X'Pert3 X-ray Diffractometer was utilized to examine the lattice structure configuration. The CuK$\alpha$ radiation and fixed power source utilized were 40 kV and 40 mA, respectively. XRD Spectrums for ZnO NSs and NTO are given in Figure 4. A hexagonal phase with space group *P*63*mc* (186) was assigned at 2 theta in the range of 10–80°, and the crystal lattice of the examined ZnO was a hexagonal structure with lattice. Debye–Scherrer equation was utilized to calculate the average of the crystallite size [39], the average crystallite size of ZnO was 25.43 nm, whereas the average crystallite size of NTO was 88.26 nm.

$$D = \frac{k\lambda}{\beta \cos \theta}, \tag{1}$$

where $D$ refers to the average crystallite size, $k$ is the Scherer's constant, $\lambda$ is the X-ray wavelength, $\theta$ is the Bragges angle, and $\beta$ is the full width at half maximum (FWHM) of the diffraction peak.

It is obvious that the crystallite size of NTO is much higher than ZnO NS where large crystallite size means that the molecules or atoms are arranged in a long-range order where NTO has good and pure intrinsic properties. The detected pattern of the NTO was monoclinic with a space group of *C*12/*m*1. The waveform pulse of NTO has half width at a high maximum (FWHM) average of

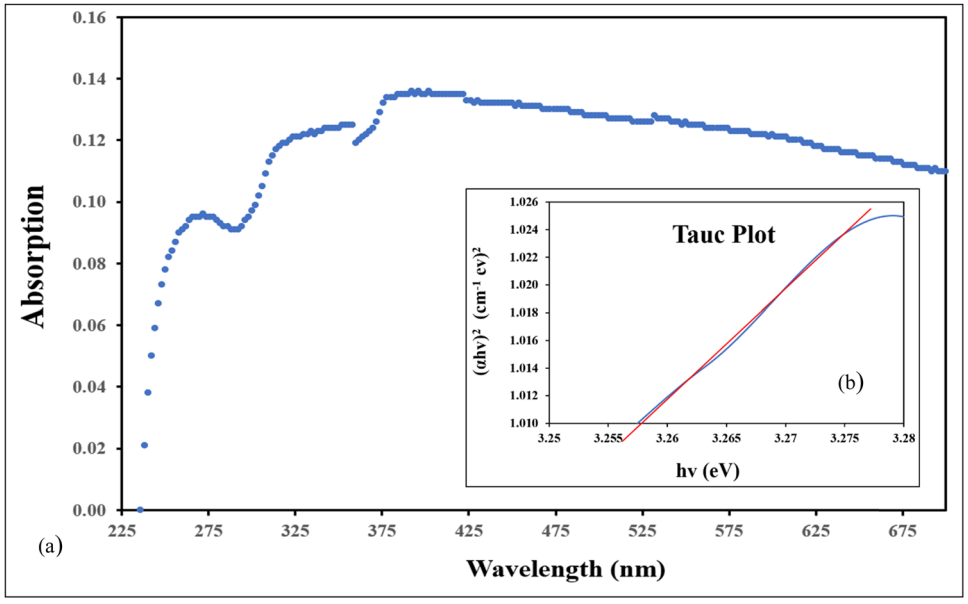


**Figure 5:** UV-Vis Absorption spectra: (a) ZnO NSs and (b) Tauc plot of ZnO NSs.

0.1 nm; in addition, the NTO spectrum peaks have narrow and sharp edges, and this indicates that the NTO have preferred electric properties and it has a high sensitivity to any change of temperature or excitations.

The detection of the energy gap ($E_g$) has been conducted to find the minimum change in energy that causes of releasing the electrons from the valence band to the conduction band. Thus, $E_g$ of ZnO and NTO were measured using ultraviolet spectrum technology as illustrated in Figures 5 and 6.

UV-Vis spectroscopy was used to examine an aqueous solution of ZnO nanosheets and NTO. The absorption of light and wavelength were measured. Tuck Plot was obtained from the absorption data $(\alpha h\nu)^{1/n}$ versus the photon energy ($h\nu$) as given in Figures 5(b) and 6(b) where a straight line extends to intersect the $x$-axis at $(\alpha h\nu)^{1/n} = 0$, where the energy gap value is determined by this intercept, and the $\alpha$ represents the absorption coefficient. The analysis of the optical absorption spectra based on the Tauc approach yielded energy gaps of ZnO NSs and NTO were 3.255 ± 0.001 and 2.23 ± 0.001 eV, respectively. The results show good electrical conductivity especially of the NTO. These facts are illustrated in Figures 5 and 6. ZnO strongly absorbs the UV- wavelength, and the standard direct band gap of zinc

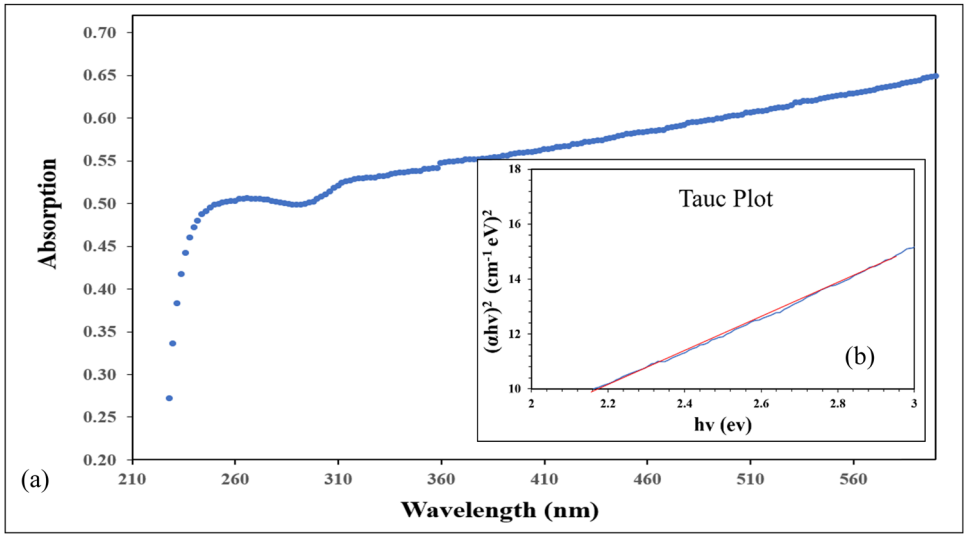


**Figure 6:** (a) UV-Vis Absorption spectra and (b) Tauc plot of NTO.

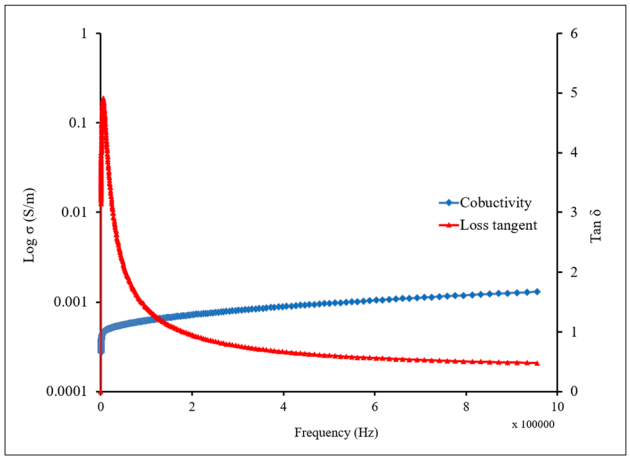


**Figure 7:** Loss tangent and conductivity of ZnO NSs–NTO.

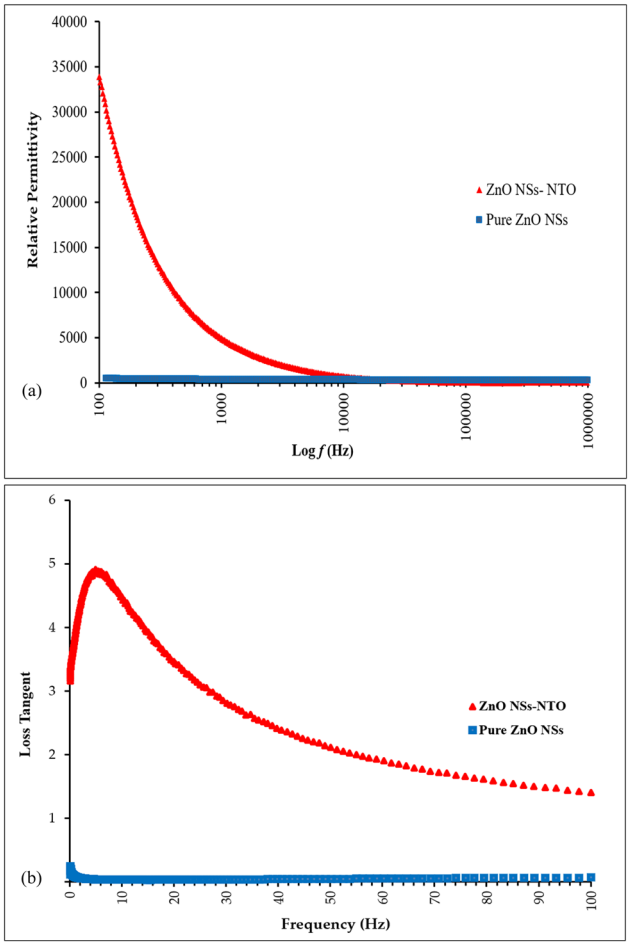


**Figure 8:** Physical properties of ZnO NSs–NTO and pure ZnO NSs: (a) dielectric constant; (b) loss tangent.

oxide is ~3.37 eV. As a result of nanosheet construction and orderly arrangement of patterns on ZnO nanosheets, there was a reduction of energy band to 3.255 (i.e., this implies that

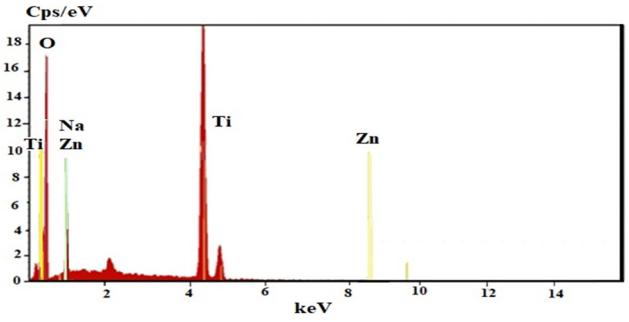


Spectrum : Acquisition

| Element | Series | Unn. C [wt.%] | Norm. C [wt.%] | Atom. C [at.%] | Error (Sigma) [wt.%] |
|---|---|---|---|---|---|
| Sodium | K-Series | 3.15 | 3.99 | 4.07 | 0.33 |
| Titanium | K-Series | 33.99 | 43.09 | 21.13 | 1.23 |
| Oxygen | K-Series | 39.69 | 50.31 | 73.85 | 8.42 |
| Zinc | K-Series | 2.06 | 2.61 | 0.94 | 0.42 |
| Total | | 78.88 | 100.00 | 100.00 | |

**Figure 9:** Surface materials identification of ZnO NSs–NTO.

ZnO nanostructures have highly mobile electrons and dense carriers), and consequently, the conductivity increases. Multiple peaks are observed in Figure 4 where that is possible for more than one electron transition to occur from a ground state into an excited state, and each peak corresponds to an electron transition (i.e., every electron has different energy and hence different wavelength).

## 3.2 Dielectric properties

The dielectric loss and conductivity of ZnO NSs–NTO were measured using an impedance analyser (model 4294A). The dielectric constant at a frequency of $10^3$ Hz was $2.249 \times 10^3$.

The dielectric constant under an alternative field is given in Figure 7. In terms of the piezoelectric characteristics, the piezoelectric coefficients are determined by calculating the permittivity and capacitance ratios. In addition, an impedance analyser uses to measure the ac-conductivity and loss tangent [40]. It is well known that in ideal cases, the dissipation of energy is zero and there is no internal heat loss under an alternating electric field. The energy dissipated in the material occurred due to the movement of the free charges and the polarization, where the dipole moves to be aligned within the applied electric field. There is a significant increase in dissipated energy at frequencies up to 5 kHz where the rate of loss tangent decreases with the increase of the frequency of electromagnetic waves up to this limit. The conductivity of NTO was measured by using the Agilest 4294A analyzer, and the conductivity was $1.2 \times 10^{-3}$ S/m at a

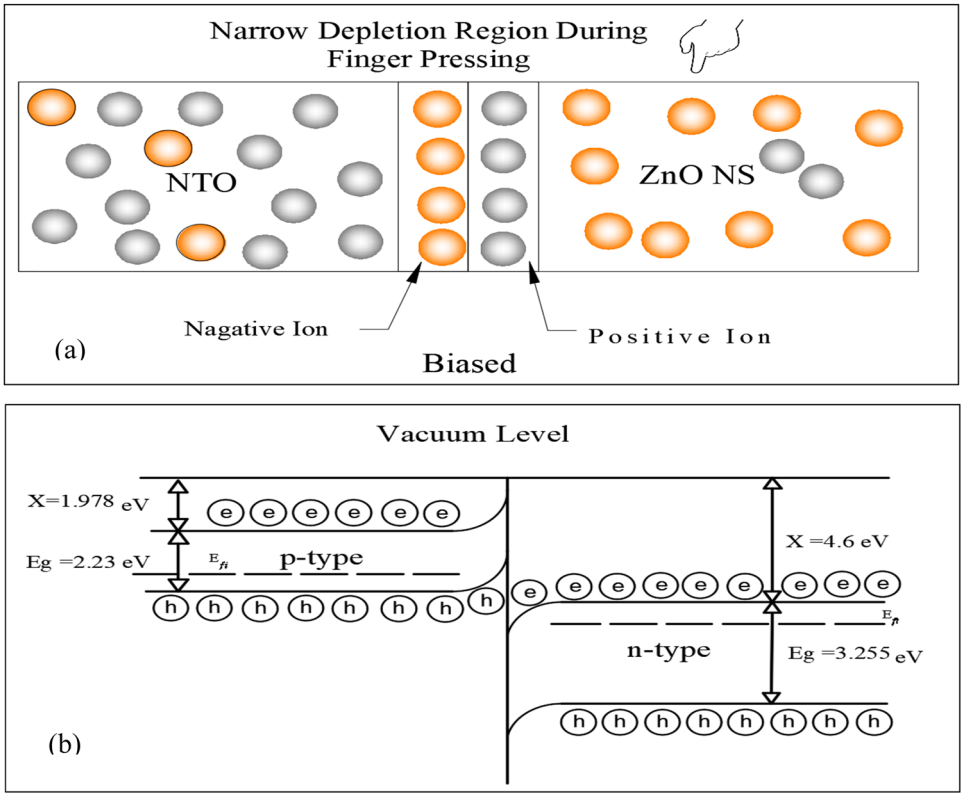


**Figure 10:** Schematic drawing finger press effect: (a) rectification and transformation of the carriers and (b) the configuration of the broken band gap under pressing.

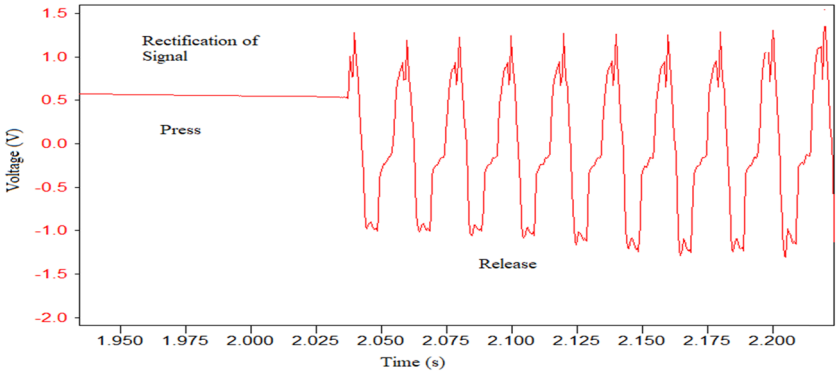


**Figure 11:** Voltage generation based on press and release at the ZnO NSs–NTO.

frequency of 1 kHz whereas the conductivity of ZnO NSs–NTO at $10^3$ Hz was $4.8047 \times 10^{-4}$ S/m, which is higher than the conductivity that measured in the prior study for the pure ZnO NSs (i.e., $10^{-5}$ S/m) [41]. High improvement of conductive properties was found due to the presence of NTO. Conductivity and loss tangent versus frequency is illustrated in Figure 8.

It was observed that loss tangent is high at low frequency; hence, this phenomenon could be attributed to the internal resistivity and due to the formation of internal heterojunction between ZnO NSs and NTO, where there is a similar behavior was detected in perovskite piezoelectric and ferroelectric materials that are known as superlattice materials [42]. On the other hand, there is the formation of Schottky–Junction and Schottky barrier resulting in increasing internal resistivity and should be taken into consideration. In Figure 8, raw ZnO NSs and ZnO NSs–NTO are compared. The results affirm that the sodium titanate assists in improving the dielectric properties whereas there is an increase of loss tangent at low frequency.

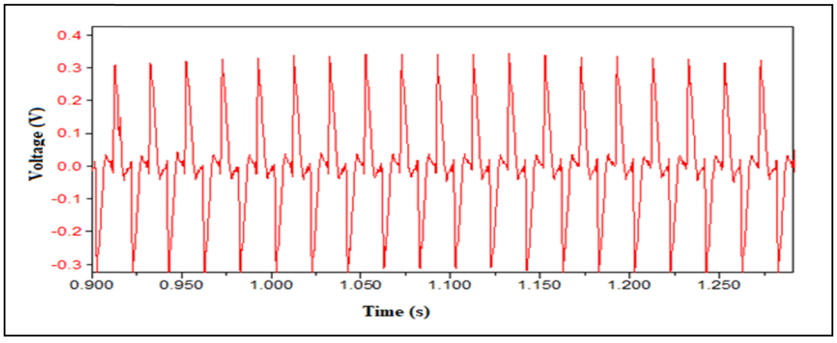


**Figure 12:** AC Voltage generation of excited ZnO NSs–NTO over cantilever beam.

## 3.3 Energy dispersive spectroscopy

The ZnO NSs–NTO components were detected by energy dispersive microscopy, and an EDS spectrum specified the exciting elements in particular points at the sample surface. The ratio between Zn, Na, Ti, and $O_2$ is detected as shown in Figure 9.

## 3.4 Energy harvesting test

The signal output is analyzed under different excitation conditions where the signal is measured after finger pressing and when the sample is held over a cantilever beam. At the moment of applying quasi-static force (i.e., at pressing moment), the fluctuation of the voltage signal

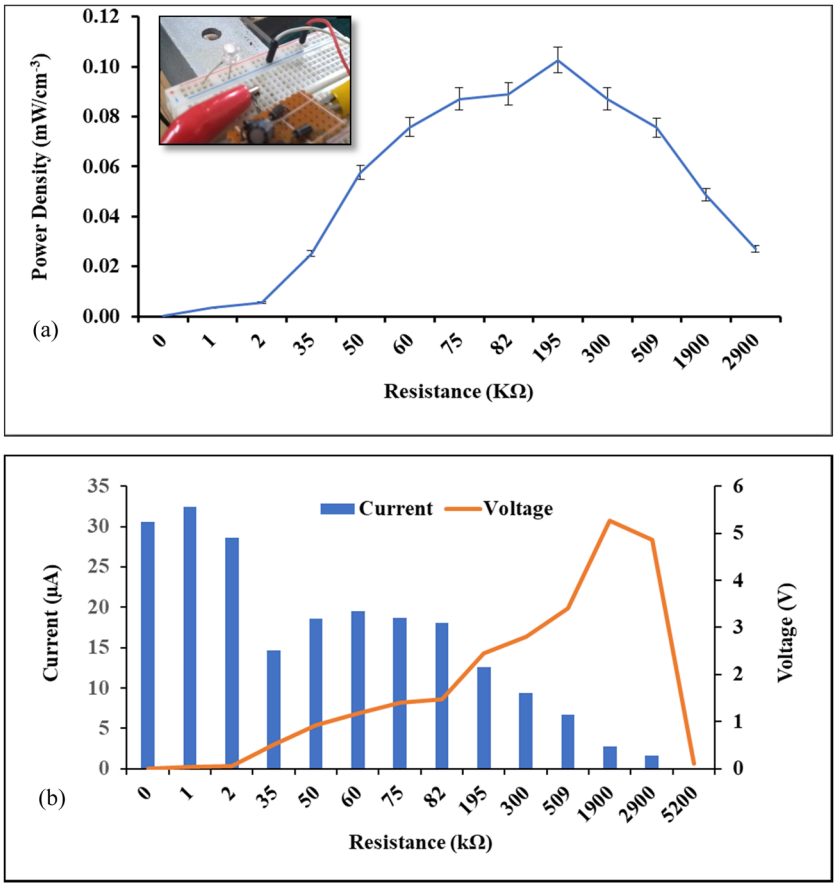


**Figure 13:** Harvesting energy over cantilever: (a) the power density of ZnO NSs–NTO that induces light up of LED diode; (b) DC voltage and current.

**Table 1:** Voltage and current measurements of ZnO NPs–NTO compared with several other studies

| ZnO nanogenerator | Voltage (V) | Current density, $I_{SC}$ (μA/cm$^2$) | Ref. |
|---|---|---|---|
| ZnO/PEDOT:PSS | 0.154 | 1.580 | [43] |
| ZnO nanowires | 2.030 | 0.107 | [44] |
| ZnO/PMMA with Schottky contact | 1.260 | 0.018 | [45] |
| GaN–ZnO–PVDF–SiO$^2$//Si | 3.100 | 0.124 | [46] |
| ZnO/Sn | 4.150 | 0.006 | [47] |
| ZnO NSs | −1.36 | 0.406 | [48] |
| ZnO NSs–$Na_2Ti_6O_{13}$ | 1.5 | 10.666 | Current study |

is rectified due to the formation of a broken heterojunction gap, and accordingly, the DC-signal could reach up to 0.5 V as given in Figures 10 and 11. There is the formation of a broken heterojunction band gap under pressing as provided in Figure 10(a and b). The broken-gap heterojunctions band is a promised structure to synthesize a high-speed switching phase. To convert the AC signal to a DC signal, a rectifier diode bridge circle has been designed, the derived electrical charge was accumulated in a capacitor, and the DC voltage was measured against a variety of external loads with load resistances in the range of (1–2,900 kΩ).

In this junction, a low-power tunnel field-constructed, the free electrons at the conduction band (ZnO NSs or n-type) diffuse across the junction forward the NTO (n-type side) and fall into holes that occupy the valence band. By virtue of the resistivity across the junction, electrons lose some energy in the form of heat. As soon as the pressing is removed, the junction band disappears and ZnO NSs–NTO regains its piezoelectricity. This fact is presented in Figure 11; the captured voltage ($V_{pa-pk}$) at finger pressing was 1.5 V. For measuring the generated AC voltage of the ZnO NSs–NTO on the excited cantilever, the sample mounted over the cantilever beam (450 mm × 40 mm × 5 mm) was excited in a frequency

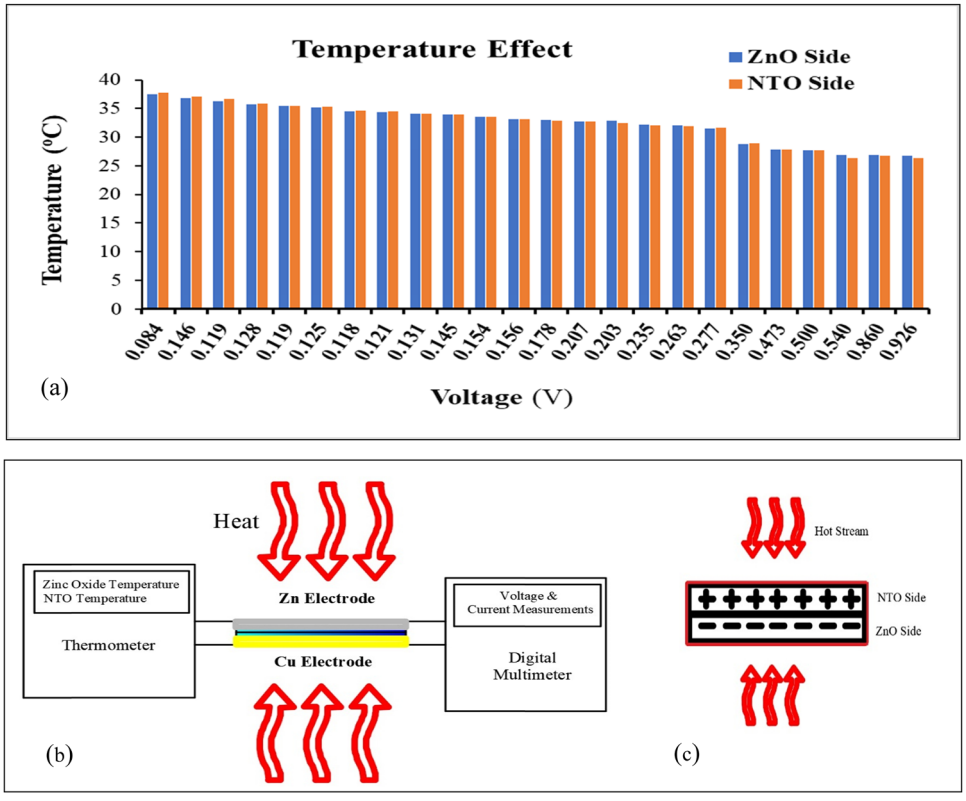


**Figure 14:** Pyroelectric property of ZnO NSs–NTO: (a) temperature versus voltage at low temperature difference (0.1–0.3°C). (b) Schematic diagram of experiment setup. (c) Signal rectification in ZnO NSs–NTO.

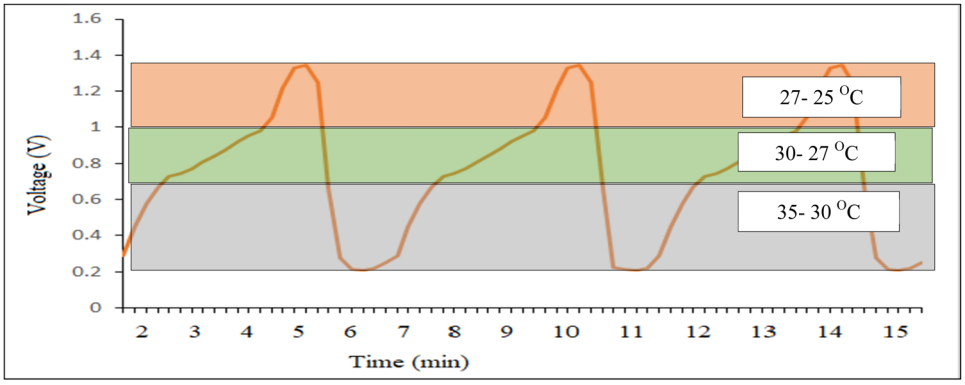


**Figure 15:** Half rectification signal.

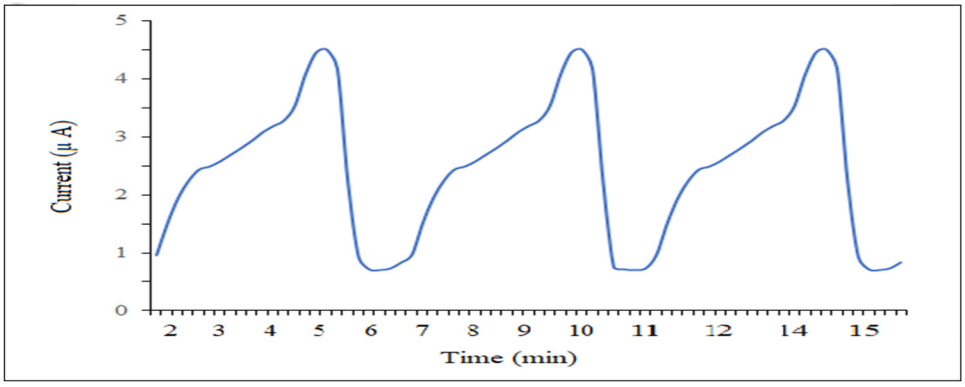


**Figure 16:** Half rectification of current.

of 30 Hz and an acceleration of 0.4 m/s$^2$. The AC voltage ($V_{pk-pk}$) was 0.6 V. High stability of voltage magnitude was verified due to the ZnO NSs–NTO being excited at a particular frequency, as shown in Figure 12. The maximum stored voltage (DC voltage) across the 100 μF capacitor was 5.3 V when the applied resistance was 195 kΩ.

The maximum power density was 0.10 ± 0.1 mW/cm$^3$ at a load resistance of 195 kΩ as provided in Figure 13.

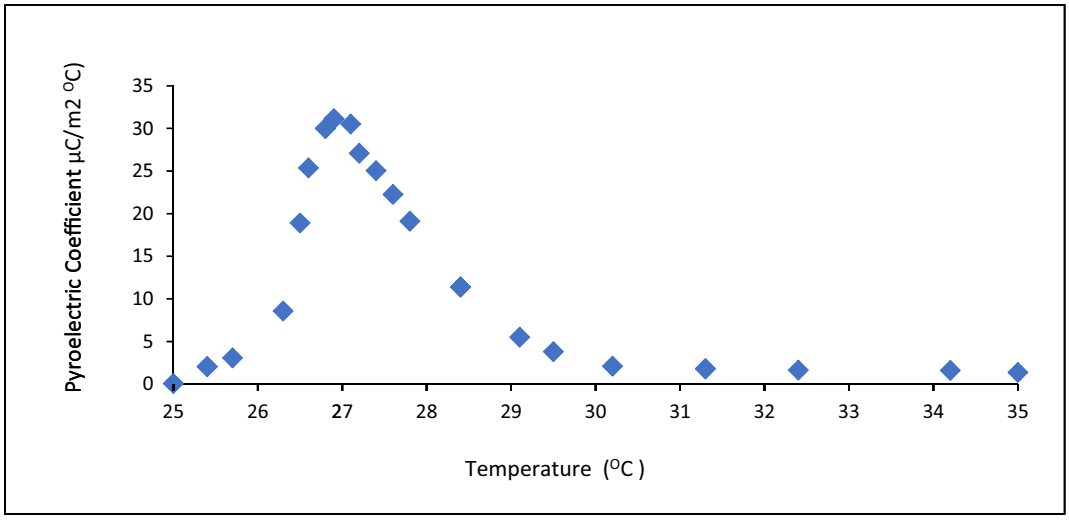


**Figure 17:** Pyroelectric Coefficient versus the change of temperature.

The rectified current is sufficient to operate LED permanently. The voltage output and current density of this work were compared to those of other nanogenerators, as shown in Table 1.

## 4 Pyroelectric behavior

The pyroelectric behavior was examined of the ZnO NSs–NTO hence, the harvester was exposed to warm air stream on both sides (i.e., ZnO NSs side and NTO side). The temperature of the Zn electrode and Cu electrode was recorded by a thermometer (model H240 and when the temperature was raised to 36°C the hot stream was removed). The reduction of the surface's temperature of the ZnO NSs–NTO versus the voltage was recorded where the temperature difference over the electrodes was in the range of (0.1–0.3°C) as provided in Figure 14(a).

Accordingly, the voltage increased upon the reduction of the surfaces' temperature as result of the development of periodical polarization or electric dipole orientation. The pyroelectric current is calculated according to the relation between the change difference over time.

$$I = \frac{\Delta Q}{\Delta t} = pA\frac{\Delta T}{\Delta t}, \tag{2}$$

where $I$ is the current, $Q$ denotes the pyroelectric of charge, $\frac{\Delta T}{\Delta t}$ is the rate of change of temperature, and $p$ represents the pyroelectric coefficient; $A$ is the electrode area. Essentially, the pyroelectric current of the nanogenerator depends on the rate of change in ($\Delta T/\Delta t > 0$). In the current study, the temperature rates for the electrodes were kept between 0.1 and 0.3°C, which is extremely small and can be ignored. In this case, the maximum current at a resistance load of 300 kΩ was 4.4 μA, the voltage, and current are given in Figures 15 and 16 where the rectified voltage rise with an offset of 0.2 V (i.e., due to there is a stored current of NTO). In fact, a dramatic increase in voltage generation was observed when the electrode temperatures varied widely as a result of the thermos sensing property effect. As a result of the heat and mechanical forces, the voltage could rise to 2 V. The pyroelectric coefficient is the change of spontaneous polarization because of the change in temperature. The pyroelectric coefficient calculates as

$$p = \frac{I_{\mathrm{p}}}{A\left(\frac{\Delta T}{\Delta t}\right)}, \tag{3}$$

where $p$ is the pyroelectric coefficient, $I_{\mathrm{p}}$ is the current, $A$ represents the harvester area. And the $\left(\frac{\Delta T}{\Delta t}\right)$ represent the ratio temperature over time. In this case, the maximum voltage was up to 1.3 V at a temperature of 26°C. The pyroelectric coefficient was calculated as shown in Figure 17. The pyroelectric coefficient reaches the maximum value at 30.51 μC/m$^2$ °C.

## 5 Conclusions

In this article, a piezoelectric was prepared from ZnO NSs and Disodium Hexa titanate. ZnO NSs–NTO provides a good dielectric constant and conductivity when compared to pure ZnO NG where the presence of a sodium titanate layer assists in increasing the generation of voltage. The dielectric constant and conductivity at $10^3$ Hz were $2.249 \times 10^3$, $4.8047 \times 10^{-4}$ S/m, respectively. A broken heterojunction bandgap could be formed under finger pressing; thus, the rectification of the signal was recorded.

The maximum generated voltage reached more than 1 V under a variety of excited loads. The maximum power density was 0.10 ± 0.1 mW/cm$^3$. It was observed a higher generation of voltage at a range of temperature of 25–27°C where the maximum pyroelectric coefficient was 30.51 μC/m$^2$ °C.

Additionally, for future work and based on the initial experimental notes, the author suggests further extension of studying the influence of temperature on energy generation in a broader range of temperatures and abrader variant of temperature for both ZnO NSs–NTO faces.

**Acknowledgements:** I would like to acknowledge all the talented people who assisted me with their expertise as I conducted this research. I also appreciate all the support that the university of Kufa has provided me.

**Funding information:** This research did not receive any specific grant from funding agencies in the public, commercial, or not-for-profit sectors.

**Conflict of interest:** The author declares no conflict of interests throughout preparing writing this paper.

## References

[1] Hammood AS, Radeef ZS, Thahab SM. Design of a piezoelectric energy harvesting device based on ZnO–$Na_2Ti_6O_{13}$ heterojunction nanogenerator. Mater Res Express. 2019;6(11):1150e9. doi: 10.1088/2053-1591/ab506f.

[2] Radeef Z, Tong CW, Chao OZ, Yee KS. Energy harvesting based on a novel piezoelectric 0.7$PbZn_{0.3}Ti_{0.7}O_3$-0.3$Na_2TiO_3$

nanogenerator. Energies. 2017;201710(5):646. doi: 10.3390/en10050646.
[3] Chen C, Sharafi A, Sun J-Q. A high density piezoelectric energy harvesting device from highway traffic – design analysis and laboratory validation. Appl Energy. 2020;269(115073):115073. doi: 10.1016/j.apenergy.2020.115073.
[4] Covaci C, Gontean A. Piezoelectric energy harvesting solutions: A review. Sensors (Basel). 2020;20(12):3512. doi: 10.3390/s20123512.
[5] bsc. Harvesting electrical charge from ambient vibration using piezoelectric materials. Edu.my. http://borneoscience.ums.edu.my/? p = 554 [cited 2022 Nov 17].
[6] Kim HW, Batra A, Priya S, Uchino K, Markley D, Newnham RE, et al. Energy harvesting using a piezoelectric "cymbal" transducer in dynamic environment. Jpn J Appl Phys. (2008)2004;43(9A):6178–83. doi: 10.1143/jjap.43.6178.
[7] Kim J, Byun S, Lee S, Ryu J, Cho S, Oh C, et al. Cost-effective and strongly integrated fabric-based wearable piezoelectric energy harvester. Nano Energy. 2020;75(104992):104992. doi: 10.1016/j.nanoen.2020.104992.
[8] Minazara E, Vasic D, Costa F. Piezoelectric generator harvesting bike vibrations energy to supply portable devices. Renew Energy Power Qual J. 2008;1(6):508–13. doi: 10.24084/repqj06.344.
[9] Edla M, Lim YY, Padilla RV, Deguchi M. An improved rectifier circuit for piezoelectric energy harvesting from human motion. Appl Sci (Basel). 2021;11(5):2008. doi: 10.3390/app11052008.
[10] Bressers S, Avirovik D, Lallart M, Inman DJ, Priya S. Contactless wind turbine utilizing piezoelectric bimorphs with magnetic actuation. Structural Dynamics. Vol. 3. New York, NY: Springer New York; 2011. p. 233–43.
[11] Rabaey JM, Ammer MJ, da Silva JL, Patel D, Roundy S. PicoRodio supports ad hoc ultra-low power wireless networking. Computer (Long Beach Calif). 2000;33(7):42–8. doi: 10.1109/2.869369.
[12] Bulusu N, Heidemann J, Estrin D. GPS-less low-cost outdoor localization for very small devices. IEEE Pers Commun. 2000;7(5):28–34. doi: 10.1109/98.878533.
[13] Lee E, Park J, Yim M, Kim Y, Yoon G. Characteristics of piezoelectric ZnO/AlN–stacked flexible nanogenerators for energy harvesting applications. Appl Phys Lett. 2015;106(2):023901. doi: 10.1063/1.4904270.
[14] Nour ES, Nur O, Willander M. Zinc oxide piezoelectric nanogenerators for low frequency applications. Semicond Sci Technol. 2017;32(6):064005. doi: 10.1088/1361-6641/aa6bde.
[15] Hu Y, Zhang Y, Xu C, Zhu G, Wang ZL. High-output nanogenerator by rational unipolar assembly of conical nanowires and its application for driving a small liquid crystal display. Nano Lett. 2010;10(12):5025–31. doi: 10.1021/nl103203u.
[16] Kamaruzaman D, Ahmad N, Rosly MA, Mamat MH. Piezoelectric energy harvesting based on ZnO: A review. 4th International Sciences, Technology And Engineering Conference (ISTEC) 2020: Exploring Materials for the Future. Arau, Malaysia: AIP Publishing; 2021.
[17] Lee Y, Kim S, Kim D, Lee C, Park H, Lee J-H. Direct-current flexible piezoelectric nanogenerators based on two-dimensional ZnO nanosheet. Appl Surf Sci. 2020;509(145328):145328. doi: 10.1016/j.apsusc.2020.145328.
[18] Zhang K-M, Zhao Y-P, He F-Q, Liu D-Q. Piezoelectricity of ZnO films prepared by sol-gel method. Chin J Chem Phys. 2007;20(6):721–6. doi: 10.1088/1674-0068/20/06/721-726.
[19] Xi Y, Song J, Xu S, Yang R, Gao Z, Hu C, et al. Growth of ZnO nanotube arrays and nanotube based piezoelectric nanogenerators. J Mater Chem. 2009;19(48):9260. doi: 10.1039/b917525c.
[20] Mansouri S, Sheikholeslami TF, Behzadmehr A. Investigation on the electrospun PVDF/NP-ZnO nanofibers for application in environmental energy harvesting. J Mater Res Technol. 2019;8(2):1608–15. doi: 10.1016/j.jmrt.2018.07.024.
[21] Manjula Y, Rakesh Kumar R, Swarup Raju PM, Anil Kumar G, Venkatappa Rao T, Akshaykranth A, et al. Piezoelectric flexible nanogenerator based on ZnO nanosheet networks for mechanical energy harvesting. Chem Phys. 2020;533(110699):110699. doi: 10.1016/j.chemphys.2020.110699.
[22] Slimani Tlemcani T, Justeau C, Nadaud K, Alquier D, Poulin-Vittrant G. Fabrication of piezoelectric ZnO nanowires energy harvester on flexible substrate coated with various seed layer structures. Nanomaterials (Basel). 2021;11(6):1433. doi: 10.3390/nano11061433.
[23] Wang ZL, Yang R, Zhou J, Qin Y, Xu C, Hu Y, et al. Lateral nanowire/nanobelt based nanogenerators, piezotronics and piezo-phototronics. Mater Sci Eng R Rep. 2010;70(3–6):320–9. doi: 10.1016/j.mser.2010.06.015.
[24] Khan A, Abbasi MA, Wissting J, Nur O, Willander M. Harvesting piezoelectric potential from zinc oxide nanoflowers grown on textile fabric substrate: Harvesting piezoelectric potential from zinc oxide nanoflowers grown on textile fabric substrate. Phys Status Solidi Rapid Res Lett. 2013;7(11):980–4. doi: 10.1002/pssr.201308105.
[25] Kaur J, Singh H. Fabrication and analysis of piezoelectricity in 0D, 1D and 2D Zinc Oxide nanostructures. Ceram Int. 2020;46(11):19401–7. doi: 10.1016/j.ceramint.2020.04.283.
[26] Wang Q, Yang D, Qiu Y, Zhang X, Song W, Hu L. Two-dimensional ZnO nanosheets grown on flexible ITO-PET substrate for self-powered energy-harvesting nanodevices. Appl Phys Lett. 2018;112(6):063906. doi: 10.1063/1.5012950.
[27] Li W, Chen R, Qi W, Cai L, Sun Y, Sun M, et al. Reduced graphene oxide/mesoporous ZnO NSs hybrid fibers for flexible, stretchable, twisted, and wearable $NO_2$ E-textile gas sensor. ACS Sens. 2019;4(10):2809–18. doi: 10.1021/acssensors.9b01509.
[28] Gupta MK, Lee J-H, Lee KY, Kim S-W. Two-dimensional vanadium-doped ZnO nanosheet-based flexible direct current nanogenerator. ACS Nano. 2013;7(10):8932–9. doi: 10.1021/nn403428m.
[29] Klingshirn C. ZnO: Material, physics and applications. Chemphyschem. 2007;8(6):782–803. doi: 10.1002/cphc.200700002.
[30] Mistewicz K. Pyroelectric nanogenerator based on an SbSI–$TiO_2$ nanocomposite. Sensors (Basel). 2021;22(1):69. doi: 10.3390/s22010069.
[31] You D, Xu C, Zhang W, Zhao J, Qin F, Shi Z. Photovoltaic-pyroelectric effect coupled broadband photodetector in self-powered ZnO/ZnTe core/shell nanorod arrays. Nano Energy. 2019;62:310–8. doi: 10.1016/j.nanoen.2019.05.050.
[32] Maurya D, Murayama M, Priya S. Synthesis and characterization of $Na_2Ti_6O_{13}$ whiskers and their transformation to (1–$x$)

$Na_{0.5}Bi_{0.5}TiO_3$-$x$$BaTiO_3$ ceramics. J Am Ceram Soc. 2011;94(9):2857–71. doi: 10.1111/j.1551-2916.2011.04444.x.
[33] Zhang Y, Hou H, Yang X, Chen J, Jing M, Wu Z, et al. Sodium titanate cuboid as advanced anode material for sodium ion batteries. J Power Sources. 2016;305:200–8. doi: 10.1016/j.jpowsour.2015.11.101.
[34] Sarkar A, Manohar CV, Mitra S. A simple approach to minimize the first cycle irreversible loss of sodium titanate anode towards the development of sodium-ion battery. Nano Energy. 2020;70(104520):104520. doi: 10.1016/j.nanoen.2020.104520.
[35] Ramírez-Salgado J, Djurado E, Fabry P. Synthesis of sodium titanate composites by sol-gel method for use in gas potentiometric sensors. J Eur Ceram Soc. 2004;24(8):2477–83. doi: 10.1016/j.jeurceramsoc.2003.07.014.
[36] Chandel S, Lee S, Lee S, Kim S, Singh SP, Kim J, et al. Hierarchically nanorod structured $Na_2Ti_6O_{13}$/$Na_2Ti_3O_7$ nanocomposite as a superior anode for high-performance sodium ion battery. J Electroanal Chem (Lausanne Switz). 2020;877(114747):114747. doi: 10.1016/j.jelechem.2020.114747.
[37] Khoo SY, Radeef ZS, Ong ZC, Huang Y-H, Chong WT, Ismail Z. Structural dynamics effect on voltage generation from dual coupled cantilever based piezoelectric vibration energy harvester system. Measurement (Lond). 2017;107:41–52. doi: 10.1016/j.measurement.2017.05.008.
[38] Geim AK. Graphene: Status and prospects. Science. 2009;324(5934):1530–4. doi: 10.1126/science.1158877.
[39] Mustapha S, Ndamitso MM, Abdulkareem AS, Tijani JO, Shuaib DT, Mohammed AK, et al. Comparative study of crystallite size using Williamson-Hall and Debye-Scherrer plots for ZnO nanoparticles. Advances in Natural Sciences: Nanoscience and Nanotechnology. 2019;10(4):045013.
[40] Babu I, van den Ende DA, de With G. Processing and characterization of piezoelectric 0-3 PZT/LCT/PA composites. J Phys D Appl Phys. 2010;43(42):425402. doi: 10.1088/0022-3727/43/42/425402.
[41] Zhang P, Hong RY, Chen Q, Feng WG. On the electrical conductivity and photocatalytic activity of aluminum-doped zinc oxide. Powder Technol. 2014;253:360–7. doi: 10.1016/j.powtec.2013.12.001.
[42] Ye Z-G, editor. Handbook of advanced dielectric, piezoelectric and ferroelectric materials: Synthesis, properties and applications. Cambridge, England: Woodhead Publishing; 2008.
[43] Briscoe J, Jalali N, Woolliams P, Stewart M, Weaver PM, Cain M, et al. Measurement techniques for piezoelectric nanogenerators. Energy Environ Sci. 2013;6(10):3035. doi: 10.1039/c3ee41889h.
[44] Zhu G, Yang R, Wang S, Wang ZL. Flexible high-output nanogenerator based on lateral ZnO nanowire array. Nano Lett. 2010;10(8):3151–5. doi: 10.1021/nl101973h.
[45] Xu S, Qin Y, Xu C, Wei Y, Yang R, Wang ZL. Self-powered nanowire devices. Nat Nanotechnol. 2010;5(5):366–73. doi: 10.1038/nnano.2010.46.
[46] Li X, Song J, Feng S, Xie X, Li Z, Wang L, et al. High-efficiency piezoelectric micro harvester for collecting low-frequency mechanical energy. Nanotechnology. 2016;27(48):485402. doi: 10.1088/0957-4484/27/48/485402.
[47] Manikandan M, Rajagopalan P, Patra N, Jayachandran S, Muralidharan M, Mani Prabu SS, et al. Development of Sn-doped ZnO based ecofriendly piezoelectric nanogenerator for energy harvesting application. Nanotechnology. 2020;31(18):185401. doi: 10.1088/1361-6528/ab6b9e.
[48] Yang A, Qiu Y, Yang D, Lin K, Guo S. Piezoelectric property comparison of two-dimensional ZnO nanostructures for energy harvesting devices. RSC Adv. 2021;11(6):3363–70. doi: 10.1039/d0ra10371c.